How Many Photons Make an Image?[*]

James Dixon[†]

CNQO, SUPA Department of Physics, University of Strathclyde, Glasgow G4 0NG, United Kingdom

(Dated: April 11, 2021)

The challenge posed by the statistical nature of photon occurrence corrupting images of low intensity light sources requires specialised image retrieval techniques. Sub-unity photocounts per pixel ratios for such methods have already been reported. This paper presents an imaging simulation inspired by quantum retrodiction methods in the literature, and analyses images resulting from low photocount measurements to reliably discriminate between sets of orthogonal and non-orthogonal images. Furthermore, statistical analysis of the measurement data for image regions of differing brightness is used to form an image in the event that an image is not uniquely identified. A sub-unity ratio of photocount per pixel is determined for image identification and the quality of image formation is found to depend on the discriminating capacity of the image regions targeted.

I. INTRODUCTION

Low intensity imaging is useful in a wide range of fields and applications, including microscopy [1] and biological applications, where light may damage an object, covert procedures and astronomical observation [2]. It is pertinent then, to ask, how many photons make an image? A regular camera forms an image from tens of thousands of photons per pixel, however, recent work has shown that images can be retrieved from as little as one photon per pixel and less [2, 3].

An image may be defined as a spatially dependent intensity structure [4]. At low intensity, quantum effects become significant and a particular issue is poisson noise, referring to the poisson distribution of photon numbers occurring about some mean, $\bar{n}$ [5]. Low light imaging of thermal sources such as astronomical structures will encounter a similar problem albeit obeying different statistics [6]. Much of the work on imaging at low light levels involves extracting an image from this noise [2]. A further challenge is the imperfect capacities of photodetectors [7]. Not all incident photons will be detected (detection efficiency) and detection is followed by detector insensitivity (dead time).

In spite of the challenges, imaging at low intensities has already demonstrated sub-unity photocount per pixel ratios by a variety of techniques [2, 8]. A short review of the literature with particular focus on retrodictive approaches will provide insight into this research area.

Morris et. al. report in their publication in Nature Communications [2], the use of a Ghost Imaging[1] setup to reconstruct an image from raw data of low photocount by optimisating for low spatial-frequency intensity variation. With a test target they obtained a reconstructed image with < 0.2 photons per pixel and applying their technique to data taken from a wasp's wing they reproduce an image with 0.45 photons per pixel. Also employing an image smoothing strategy, Agnew et. al. writing in Scientific Reports, present an image reconstruction algorithm effective for number of photons detected per pixel of the order of unity [3].

Since the late nineties Barnett and collaborators have established a theory of state retrodiction - retrodiction being temporally backwards prediction (Sec.II B) [8–11]. They write in Optics Communications [9] on using retrodiction to investigate a pre-measured state given measurement by an imperfect detector. Instead of describing the state of light in terms of its preparation and then the statistics of measurement outcomes, their approach is to 'work back' from measurement by an imperfect detector to determine the pre-measured state. They find that this retrodicted state is a mixed state representing a lack of information relative to finding a pure state. This, they explain, is due to incorporating the detector imperfections into the retrodiction.[2] In 1999, they demonstrated a relationship between predictive and retrodictive use of quantum mechanics, representing the pre-measured state with a density operator [10]. Then in Optica (2015) [11], Bayesian statistical techniques were applied to low photocount data to retrodict intensity values at each detector. Building on this, Barnett et. al. (2017), use quantum retrodiction to develop an algorithm for denoising and determining intensities at detectors with low photon number data [8]. Their objective was to determine the pre-measurement state given a particular set of low photocount data subject to Poisson noise. They do this employing Bayesian inference, to retrodict probability distributions for intensities at each detector. Their use of retrodiction takes account of the detection (or not) of a photon and the activity of other detectors around it. The

---

[1] Ghost Imaging is a technique in quantum imaging. It uses entangled pairs of photons, one of which probes an object and the other does not, that reach different detectors. Their combined output is used to construct the image [5].

[2] They note, interestingly, that using such a process in quantum telecommunication, in which a prepared state is sent to a receiver and the receiver retrodicts the transmitted state, wavefunction collapse takes place when the receiver measures, in the senders perspective, and for the receiver when the sender prepares the state.

image is then constructed from the retrodicted distributions, which also allow for evaluation of the reliability of the image determination. Their algorithm applied to simulated data recovers the image with an average of 0.2 counts per pixel.

As outlined above, reducing photocounts whilst optimising image extraction has produced impressive results, but photocounts can also be used to distinguish between images [4, 12]. Images are said to be orthogonal if it is possible for a single photon to distinguish between them [13]. For example, Broadbent et. al. (2009) distinguish 2 orthogonal images encoding image information onto a single photon[12]. However, non-orthogonal images may also be distinguished by low photocounts, though the discrimination may be less reliable [14]. In the field of facial recognition, images can be identified quickly by pattern recognition from a predefined set of images to decide between [15]. A set of orthogonal images decomposed of a library of faces, so-called 'eigenfaces', are amalgamated to decide on or form the image transmitted by low photocounts. Ideally, appropriate weighting of 'eigenfaces' can reconstruct any face. With these considerations, the strategy of this work for image identification from low photocount follows. Given a set of possibly transmitted images, a photon arriving at a detector, suggesting a bright region of the image, will exclude from identification any image expected to be dark in this region. This requires that the measured image is a member of the basis set of expected images with orthogonal regions. That is, image regions which are mutually exclusive. In this way, one photon can differentiate two images and N photons, 2^N images [4]. Further, regions of images of different brightnesses will have differing expectation values for number of photons arriving. Put simply, brighter regions expect to receive more photons and darker regions less. In this way, unexpectedly deviating photocount statistics can be used to distinguish between non-orthogonal images and the magnitude of deviation can be used to weight images in composing a likely received image, should an image not be uniquely identified.

Inspired by the literature on quantum retrodiction and the concepts of image orthogonality and eigenfaces, it is the aim of this paper to explore, theoretically and computationally, the strategy outlined above for low photocount image identification to reduce the ratio of detected photons to number of pixels, Q. Section II will introduce the assumed setup and parameters as well as providing the theoretical basis for image retrodiction. In Sec. III, a simulated photodetection and image retrodiction algorithm with the capacity to reliably identify a transmitted image from low photocount is detailed. The software was developed entirely on *Matlab* by the author of this paper. The results are presented in Sec. IV, including a sub-unity value for Q for identified images. In the case that no image is uniquely identified, a weighted formation of an image superposed of the set of base images is offered. The response to a transmitted image that is not a member of the basis set is also provided. A discussion of the findings follows (Sec. V) and concluding remarks are made in Sec. VI.

II. BACKGROUND AND THEORY

A. Assumed Apparatus Parameters and Light Source

Generally, single photon detectors rely on the photoelectric effect. As a single photon will stimulate the emission of one photoelectron, they must be designed with an internal signal amplifying mechanism in order to be recognised by electronic circuits [7, 16]. One type of detector frequently employed in single photon detection are Single Photon Avalanche Diodes (SPADs). These consist of a p-n junction subject to a potential greater than breakdown voltage allowing a single incident photon to trigger an electrical response [7]. However, multiple simultaneously incident photons will not trigger a distinguishable output pulse; once activated, a detector is insensitive for a period called the dead time. Increasing photon detection rates depends on reducing the dead time and rates of up to several MHz are possible making them commonly used in photon counting experiments [7]. The most important parameter in photocounting experiments is the ratio of the number of output pulses to incident photons, the detection efficiency, η, which is often 0.5 or lower [7, 17]. A value $\eta = 0.5$ is assumed for this work. Other complicating features of SPADs, such as dark count and after-pulsing will be excluded. Furthermore, SPADs can be arranged in arrays, with one detector corresponding to one pixel to form an image detector [17]. This will be the assumed detection apparatus underpinning the following work. The key features are that the detection output is binary, either a 'click' or 'no-click', regardless of the number of incident photons, with a detection efficiency of $\eta = 0.5$.

This work will assume a single mode of a coherent light source. Coherent states, $|\alpha\rangle$, are defined as the eigenstates of the annihilation operator [6],

$$\hat{a} |\alpha\rangle = \alpha |\alpha\rangle. \tag{1}$$

From which they can be derived as a superposition of number states $|n\rangle$,

$$|\alpha\rangle = \exp\left(-\frac{|\alpha|^2}{2}\right) \sum_{n=0}^{\infty} \frac{\alpha^n}{\sqrt{n!}} |n\rangle, \tag{2}$$

with mean photon number $\bar{n} = \langle\alpha|\hat{n}|\alpha\rangle = |\alpha|^2$. From the usual definition of probability in quantum mechanics, the probability of a particular number of photons

$$P(n) = |\langle n|\alpha\rangle|^2 = \exp(-\bar{n})\frac{\bar{n}^n}{n!}. \tag{3}$$

This is a poissonian distribution with spread Δn and relative fluctuations $\frac{\Delta n}{\bar{n}} = \frac{1}{\sqrt{\bar{n}}}$. This becomes significant

for low intensity light, concealing the value of $\bar{n}$ (poisson noise).

A maximum intensity $\bar{m}$ is assumed to be permitted in the system and as a single mode source is assumed, $\bar{n}$ is the intensity or brightness of the source.

B. Retrodiction

Prediction can be represented as $P(A|B)$, the probability that event A occurs given that event B occurred, and is a temporally forward propagating concept. Retrodiction, $P(B|A)$, is then the converse, propagating backwards in time. This concept is useful in imaging, where we want to discern the intensity of light responsible for a set of binary measurements, such as might result from the assumed setup in this work. Quantum retrodiction has the defining characteristic of assigning a pre-measured state given a measurement. [8]. This work is concerned with retrodicting the brightness of the pre-measured state, $P(\bar{n}|\checkmark)$ or $P(\bar{n}|\times)$. These are the probabilities that a particular brightness of light, $\bar{n}$, was responsible for a detector click $\checkmark$ or no-click $\times$.

Prediction and retrodiction are related by Bayes' Theorem [18] , expressed in this context,

$$P(\bar{n}|d) = \frac{P(d|\bar{n}) \cdot P(\bar{n})}{\sum_{\bar{n}=0}^{\bar{m}} P(d|\bar{n}) \cdot P(\bar{n})} \qquad (4)$$

where $d = \checkmark, \times$. $P(\bar{n})$, referred to as the prior, is the probability that a particular brightness of light illuminated the detector. The weighted sum in the denominator,

$$\sum_{\bar{n}=0}^{\bar{m}} P(d|\bar{n}) \cdot P(\bar{n}) = P(d), \qquad (5)$$

is the total probability of detection d.

C. Initial State - Prior

Initially, there is no information about the brightness of light on shining on the detector and a reasonable prior is a uniform distribution. This may be used to express a mixed state with density operator,

$$\hat{\rho} = \frac{1}{\bar{m}+1} \sum_{\bar{n}=0}^{\bar{m}} |\psi_{\bar{n}}\rangle \langle \psi_{\bar{n}}| \qquad (6)$$

For a coherent source of discrete integer $\bar{n} = 0, ..., \bar{m}$, the state before any measurement is taken is

$$\hat{\rho}_\alpha = \frac{1}{\bar{m}+1} \sum_{|\alpha|^2=0}^{\bar{m}} |\alpha\rangle \langle \alpha|$$

$$= \frac{1}{\bar{m}+1} \sum_{\bar{n}=0}^{\bar{m}} \sum_n \sum_{n'} e^{-\bar{n}} \frac{\alpha^{*n} \alpha^{n'}}{\sqrt{n!}\sqrt{n'!}} |n'\rangle \langle n| . \qquad (7)$$

For this work the non-diagonal terms do not matter and $\hat{\rho}_\alpha$ is simplified

$$\hat{\rho}'_\alpha = \frac{1}{\bar{m}+1} \sum_{\bar{n}=0}^{\bar{m}} \sum_n e^{-\bar{n}} \frac{\bar{n}^n}{n!} |n\rangle \langle n| . \qquad (8)$$

D. Predictive Probabilities

In order to calculate the retrodiction $P(\bar{n}|d)$ we need the predictive probabilties $P(d|\bar{n})$ in addition to the prior. Given that the relative fluctuations of photon number are increasingly significant at low intensities, this must be accounted for in determining the predictions for the SPAD behaviour. The predictive probabilities for a $d = \checkmark$ or $d = \times$, given a vacuum state or a coherent state with any $\bar{n}$ possible for the system $P(d|\bar{n})$, are determined with the following considerations.

The probability that a detector does not click given zero photons arriving at the detector is $P(\times | |0\rangle) = 1$ and the complement, $P(\checkmark | |0\rangle) = 0$. If one photon arrives, the click probability is the detector efficiency, $P(\checkmark | |1\rangle) = \eta$ and complementarily $P(\times | |1\rangle) = 1 - \eta$. The arrival of n photons at once constitutes n independent events and the no-click[3] probability is then the complement of the detector efficiency raised to the power n, $P(\times | |n\rangle) = (1-\eta)^n$. This gives the general form with the complement, $P(\checkmark | |n\rangle) = 1 - (1 - \eta)^n$.

The source of light is a mixed state (Sec. II C). So, to find $P(\times | |\alpha_{\bar{n}}\rangle)$, the statistical quantum mechanics formalism can be employed. A no-click detection operator can be represented,

$$\hat{\Pi}_\times = \sum_n (1-\eta)^n |n\rangle \langle n| , \qquad (9)$$

yielding the probability that the detector did not click given the incidence of n photons.

The total probability for a no-click event is the expectation value of the no-click detection operator in the mixed state $\hat{\rho}'_\alpha$ (Eq. (8)),

$$P_\alpha(\times) = \langle \hat{\Pi}_\times \rangle = Tr\big(\hat{\rho_\alpha}' \hat{\Pi}_\times\big). \qquad (10)$$

This gives

$$\sum_m \langle m| \frac{1}{\bar{m}+1} \sum_{\bar{n}=0}^{\bar{m}} e^{-\bar{n}} \frac{\bar{n}^n}{n!} |n\rangle \langle n| \sum_{n'} (1-\eta)^{n'} |n'\rangle \langle n'|m\rangle , \qquad (11)$$

which reduces to

$$P_\alpha(\times) = \frac{1}{\bar{m}+1} \sum_{\bar{n}=0}^{\bar{m}} e^{-\eta\bar{n}}. \qquad (12)$$

————

[3] Consideration of $P(\checkmark | |n\rangle)$ runs into the challenge of computing the union of unspecified numbers of non-mutually exclusive events

See Appendix A for full derivation. Recalling Eq. (5), the total probability for no click

$$P(\times) = \sum_{\bar{n}} P(\times | |\alpha\rangle_{\bar{n}}) \cdot P(|\alpha\rangle_{\bar{n}}). \qquad (13)$$

This is the sum of the products of the predictive probability and the prior for each possible $\bar{n}$.

Comparing Eq.s (12) and (13), the prior is the uniform distribution,

$$P(|\alpha\rangle_{\bar{n}}) = \frac{1}{\bar{m}+1} \qquad (14)$$

and the predictive probabilities are,

$$P(\times | |\alpha\rangle_{\bar{n}}) = e^{-\eta\bar{n}}, \qquad (15)$$
$$P(\checkmark | |\alpha\rangle_{\bar{n}}) = 1 - e^{-\eta\bar{n}}. \qquad (16)$$

E. Prior Update

With the predictive probabilities and the prior, $\bar{n}$ can be retrodicted with Eq. (4), Bayes' Theorem. Calculating $P(\bar{n}|d)$ for each possible $\bar{n}$ the prior can be replaced with a measurement evidenced update. Consider an example, a single detector is illuminated by a source of 10 possible brightness levels including the vacuum state. The prior update from a $\checkmark$ and $\times$ measurements are shown in Fig.s 1 and 2. The prior can then be interpreted as an image by finding the brightness B as the expectation value of $\bar{n}$, in the prior.

$$B = \langle \bar{n} \rangle = \sum_{\bar{n}=0}^{\bar{m}} \bar{n} P(\bar{n}) \qquad (17)$$

Here, $B = 0$ is a black pixel, representing the vacuum state and $B = \bar{m}$, white, the brightest state possible. Given consecutive measurements as time progresses, the prior can be repeatedly updated, a process equivalent to learning, known as Bayesian inference. Over enough time the prior is refined and converges as a peak at the intensity of light incident on the detector. This is seen in Fig. 3, which displays the evolution of the prior for 120 measurements, corresponding to 120 time-steps.

F. Multiple detectors

To retrodict an image, consider an array of detectors as assumed in Sec. II A. The distribution of retrodictions for all $\bar{n}$ at a detector $D^{(i)}$ must be calculated (sub/superscript i indicates events at a particular detector). Now, a particular $\bar{n}_i$ can occur at $D^{(i)}$ for every possible $\bar{n}$ at all other detectors. So, the total probability that a particular state illuminated a particular detector given a detection, $P_T^{(i)}(|\alpha_{\bar{n}}\rangle^{(i)} | d^{(i)})$, is then; the sum of all possible combinations of products of retrodictions for all other detectors, multiplied by $P^{(i)}(|\alpha_{\bar{n}}\rangle^{(i)} | d^{(i)})$.
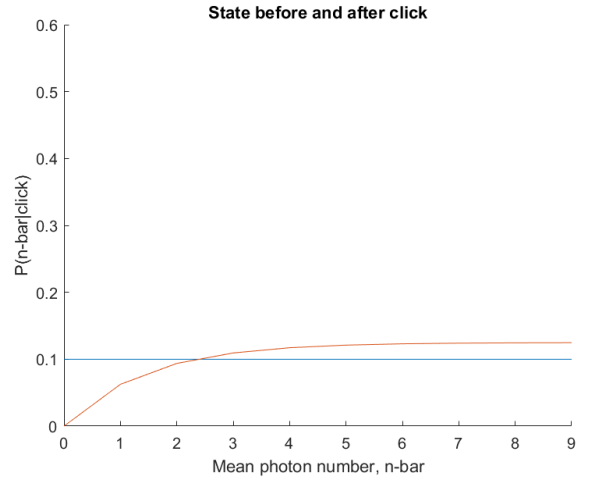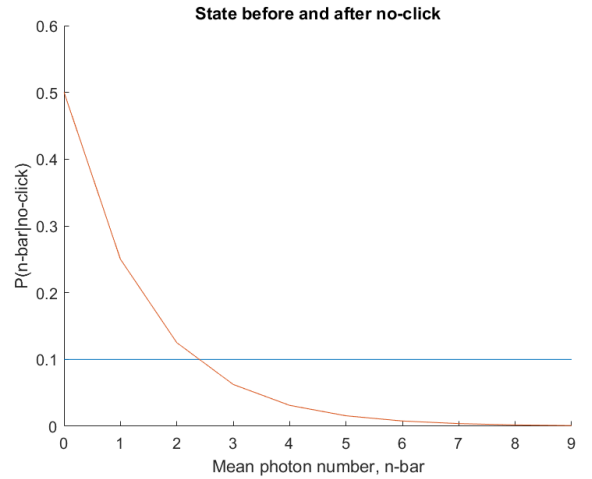

FIG. 1: State before (blue) and after (red) a single retrodictive update. The initial state is a uniform distribution representing the lack of knowledge of $\bar{n}$. This becomes a brighter state, a higher $\bar{n}$ being more likely, following a photocount. It is now impossible that the state is a vacuum state.

FIG. 2: State before (blue) and after (red) a single retrodictive update. The initial state is a uniform distribution representing the lack of knowledge of $\bar{n}$. This becomes a darker state, a lower $\bar{n}$ being more likely, following no photocount.

To clarify, consider this example, take three detectors and three light intensities including the vacuum state, and a set of detections $\vec{d} = [\times, \checkmark, \times]$. The probability that the detectors were illuminated by states of particular $\bar{n}_i$ is,

$$P_{\bar{n}_1\bar{n}_2\bar{n}_3} = P\left(|\alpha\rangle_{\bar{n}_1}^{(1)}, |\alpha\rangle_{\bar{n}_2}^{(2)}, |\alpha\rangle_{\bar{n}_3}^{(3)} | \times^{(1)}, \checkmark^{(2)}, \times^{(3)} \right). \qquad (18)$$

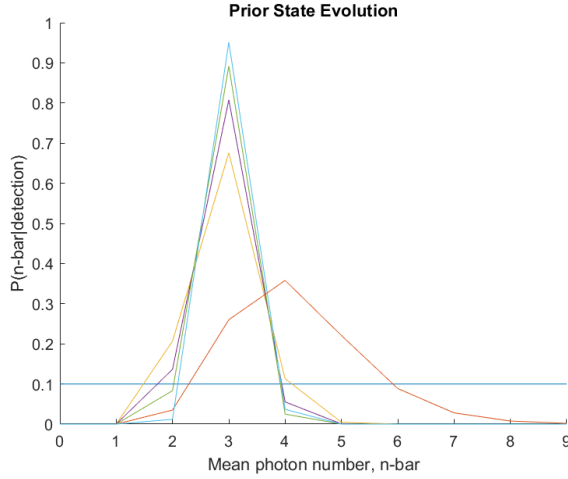This can be factored, as the events at the individual de-

FIG. 3: With simulated light detections for $\bar{n} = 3$ at one detector ($\eta = 0.5$), the prior state is seen to evolve over 120 time-steps, 6 evenly spaced steps are displayed. The initial state is the horizontal line, representing the initial lack of knowledge of brightness. The plots then evolve with a Bayesian update of the prior, which is seen to become increasingly sharp at $\bar{n} = 3$.

tectors are independent,

$$P_{\bar{n}_1 \bar{n}_2 \bar{n}_3} = P(|\alpha\rangle^{(1)}_{\bar{n}_1} |\times\rangle) \cdot P(|\alpha\rangle^{(2)}_{\bar{n}_2} |\checkmark\rangle) \cdot P(|\alpha\rangle^{(3)}_{\bar{n}_3} |\times\rangle). \quad (19)$$

Now, the vacuum state arriving at $D^{(1)}$ can occur for all combinations of intensities on $D^{(2)}$ and $D^{(3)}$. So, the probability of the vacuum state being incident on $D^{(1)}$ is the sum of all these combinations multiplied by $P^{(1)}(|0\rangle |\times\rangle)$.

$$P_T(|0\rangle^{(1)} | \times^{(1)} \cap \checkmark^{(2)} \cap \times^{(3)}) = P_0^{(1)} \sum_{\bar{n}_2=0}^{\bar{m}} \sum_{\bar{n}_3=0}^{\bar{m}} P_{\bar{n}_2 \bar{n}_3} \quad (20)$$

In general, for an array of N detectors, the total retrodiction for some $\bar{n}_i$ at detector $D^{(i)}$ is,

$$P_T^{(i)}(\bar{n}_i) = P^{(i)}(\bar{n}_i | d^{(i)}) \sum_{\bar{n}_2} \sum_{\bar{n}_3} ... \sum_{\bar{n}_N} P_{\bar{n}_2 \bar{n}_3 ... \bar{n}_N} \quad (21)$$

In this manner, a new prior is calculated for all $\bar{n}$ at each detector. The resulting distribution of the mixed state at each detector can then be used to obtain B, according to Eq. (17), or as the prior to be combined with further evidence in another Bayesian update. Sufficient detection events and update iterations will allow for an accurate retrodiction of the spatial intensity structure responsible for the pattern of observed clicks and no-clicks.

III. METHODS

A. Retrodiction Simulation

1. Detection Simulation

An image to be transmitted was represented by a matrix with integer elements, representing $\bar{n}^{(i)}$ of the incident light, located at corresponding positions to detectors in an array. This matrix could be set manually or, any Portable Network Graphics (PNG) file can supplied. In this case, the file is converted to a 50×50 matrix of 'double' data type. As PNG files have 256 brightness levels, the value at each pixel was mapped to a scale from 0 to $\bar{m} = 5$, where 0 is a black pixel and 5 a white. The mapping formula is,

$$e' = e \cdot \frac{\bar{m}}{256} \quad (22)$$

where e is the matrix element and e' is its mapped value, which was rounded to the nearest integer. Choosing $\bar{m} = 5$ or less significantly reduced computation time and is in accordance with an assumed low intensity. For each detector in the assumed SPAD array, a click was generated if a random number $r > P(\times|\bar{n}^{(i)}) = e^{-\eta \bar{n}^{(i)}}$ and a no-click otherwise. Thus, a set of detections $\vec{d}$, one at each detector, was produced in each time-step. A time step can be considered the length of the dead time of the detector. So in a step, each detector will return a binary measurement - if a detection occurs the detector must reset and this begins the next time step. Detection events at all detectors run in parallel.

2. Image Retrodiction

An image retrodiction simulation was developed in accordance with the assumptions and theoretical considerations outlined in Sec. II. That is, an array of SPADs, of detection efficiency $\eta = 0.5$, illuminated by some low intensity, single mode, coherent light source transmitting an image, with a maximum intensity, $\bar{m} = 5$. At the core of the algorithm is Bayes' theorem as considered for multiple detectors, Eq. (21). This is supplied the prior distribution for $\bar{n}$, Eq. (14) and the detector behaviour predictions, given a simulated set of clicks, Eq. (16), and no-clicks, Eq (15), for each detector generated as explained in the previous section. One set of detections and corresponding update of the prior is one time-step, so running over multiple time-steps simulates Baysian inference of the image over time. The schematic in Fig. 4 depicts the image retrodiction algorithm.

Once the algorithm has run for the set number of time steps, a brightness B is calculated at each pixel according to Eq. (17) with the computed prior, $P(\bar{n})$. This comprises a matrix, which is displayed as the measured image.
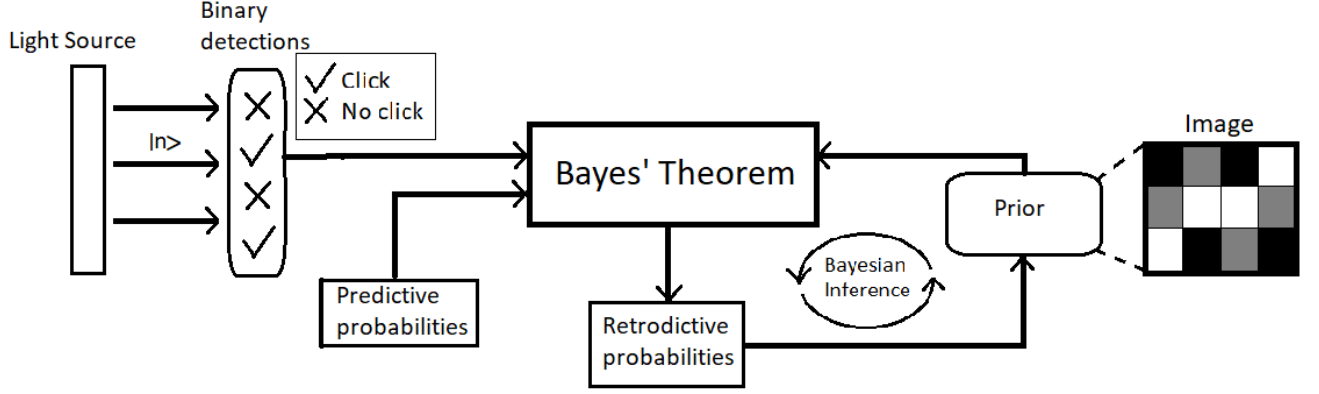
FIG. 4: Schematic of image retrodiction algorithm.

For a demonstration of image retrodiction see Sec. IV and more comprehensively in Appendix C. One time-step was sufficient to realise most results in this work, occasionally up to 3 were required. The prior distributions determined by more time steps could be of use for more refined applications of the techniques that will be presented. Equivalent theoretical considerations for a thermal/chaotic source of light as those given in Sec.s II D and II E are available in Appendix B. The image retrodiction software may be applied for such a source. However, due to the greater spread in the geometric distribution governing the photon statistics, successful image retrodiction required far greater numbers of photons. The intention of this work is to find the lowest value for the ratio of photocounts to pixels Q, so the thermal source was not considered in determining Q.

B. Image Library

Libraries of images to be transmitted and identified were assembled. One contained simple, black and white letters of the alphabet, produced with Microsoft Paint. These were designed to all have overlapping black on white regions rendering them orthogonal for discrimination. Another, portraits of 20 influential figures in physics (Fig. 5) comprising both orthogonal and non-orthogonal images. They were all available under creative commons license. Every image was converted to a PNG file and, for the portraits, cropped to show only head and shoulders with the faces in approximately the same region of the image. To reduce the computational load, the images were formatted as described in Sec. III A 1. A program was developed to record the matrix location indices of each brightness level of each library image as ".txt" files for computational efficiency.

FIG. 5: Portrait library images. Images were available under Creative Commons License and adapted as described in Sec.s III A 1 and III B. From top left Aristotle, N. Bohr, S. Hawking, E. Noether, L. Bolzmann, M. Curie, J.C. Maxwell, R. Penrose, L. de Broglie, P. Dirac, J. von Neumann, M. Planck, A. Einstein, R. Feynman, I. Newton, E. Rutherford, C. Gauss, S. Hossenfelder, E. Schrodinger, N. Tesla [19–38]

C. Image Discernment

With the image retrodiction software and a library of possibly received images, referred to as the basis, a procedure was developed to identify a basis image from the measured image of low photocount. To do this, as previ-

ously indicated, pixels in the measured image that turned brighter were compared to each black pixel of each base image in turn. If a base image pixel was black where the measured pixel became brighter, the image was excluded from the basis as, $P(\checkmark|\bar{n}=0)=0$ by Eq. (16). In practice, this was sufficient to identify letters. For the portrait basis, this left at least 7 of 20 base images. To decide between the remaining images another criteria for exclusion was instigated. Considering the pixels with darkest shade of grey, '$G1$', corresponding to $\bar{n}=1$, the probability of a pixel turning brighter, receiving a click measurement, according to Eq. (16) with $\eta=0.5$, is $P(\checkmark|1)=1-e^{-0.5}$. A basis image has N_{G1} $G1$ pixels and the expectation for clicks at $G1$ pixels, if that base image was measured, is $\langle N_{G1}(\checkmark)\rangle = P(\checkmark|1)\cdot N_{G1}$. The number of clicks measured, $N_{G1}(\checkmark)$, is poissonianly distributed about $\langle N_{G1}(\checkmark)\rangle$ with standard deviation $\sigma = \sqrt{\langle N_{G1}(\checkmark)\rangle}$. Images were excluded if $|N_{G1}(\checkmark)-\langle N_{G1}(\checkmark)\rangle| > 2\sigma$, the 95% confidence interval. For the shades with which this procedure was used, all images had more than 100 pixels and the Normal distribution confidence margins apply suitably. As expected, this still resulted in more than 1 base image remaining in some instances and the further exclusion condition was added, $|N_{G4}(\checkmark)-\langle N_{G4}(\checkmark)\rangle| > 2\sigma$. This eliminated any incorrect images remaining in the basis (Sec. IV). The $G1$ and $G4$ pixels were targeted as they were expected to contrast images more reliably. Trial and error supported this decision and subsequent data collection justified it (Table I).

D. Image Formation

In some preliminary trials with the portrait library, all images were excluded by the double 2σ exclusion procedure. It was also deemed possible that more than one image might remain. In these cases, procedures were developed to form an image as a weighted sum of base images. The intention was that suitable interpretation of the measured data, in weighting non-excluded base images, might generate an image similar to the transmitted image. The 'eigenface' concept was inspirational in developing this protocol.

The weighting of images was calculated as follows. Considering $G1$ again, the difference between the number of brighter pixels measured at corresponding $G1$ locations on a base image and the expected number of brighter $G1$ pixels for that image was divided by the standard deviation of the expected number. This was taken as the measure of dissimilarity between the measured image and that image.

$$Dissimilarity = \frac{|N_{G1}(\checkmark) - \langle N_{G1}(\checkmark)\rangle|}{\sqrt{\langle N_{G1}(\checkmark)\rangle}} \quad (23)$$

This gives larger scores for images with an expected value further from the number measured. It further reduces that score by the magnitude of the standard deviation,
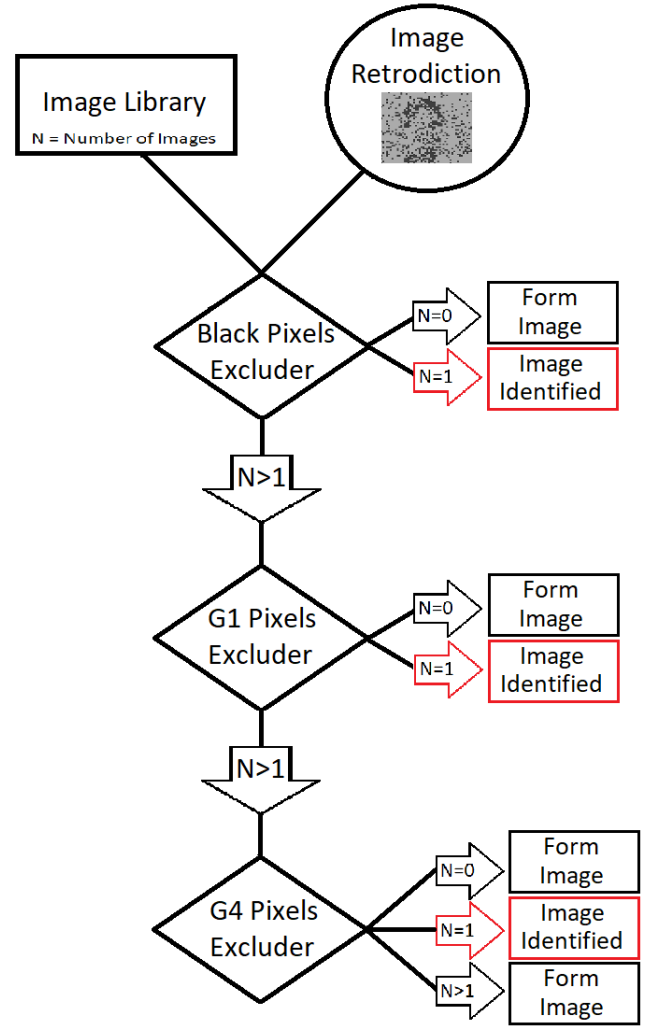

FIG. 6: Schematic outline of image deciding algorithm. Inputs are the image library, with N images, and the retrodicted image measurement. Exclusion procedures remove orthogonal or unlikely images until the image is discerned, N=1, or a possible image can be formed.

as brighter shades or images with larger numbers of pixels of that shade would be expected to provide measurements that deviate further from the mean in absolute terms. The dissimilarity score is inverted to become a similarity score. If the basis has more than 3 images remaining, the dissimilarity for each image was divided by the highest dissimilarity score, so the most dissimilar image had a score of 1. The similarity for each image was then the dissimilarity score subtracted from 1 and the most dissimilar image is discarded. If the basis had 3 or less images remaining, the similarity score was taken as the reciprocal of the dissimilarity score. The similarity scores were normalised for use as a weighting distribution for the base images in image formation. The 2 different conversions were an optimisation of the quality of formed images by trial and error of methods.

The following procedure is outlined schematically in Fig. 6.

In the case that all base images are excluded by comparison with black pixels, an image is formed as a weighting of the entire library of images. This does not occur for this set of library images.

In the case that more than one base image remained following all exclusion tests, the remaining images were weighted as described above.

If all images were excluded for violating the double 2σ exclusion, two cases were distinguished. The first, that $G1$ pixel comparison had eliminated all images. Here the weighting procedure was used considering all images remaining after the black pixel exclusion. As the transmitted image had been excluded by $G1$ data, this would not provide appropriate weighting for the transmitted image, so the weighting was determined by the $G2, G3$ and $G4$ shades. The second case is that the combination of $G1$ and $G4$ exclusion eliminated all images. In this case, an image was formed as a weighting of the images left following exclusion by the black and $G1$ shades. Here, the data at the $G4$ images was outwith 2σ, so the shades $G1, G2$ and $G3$ were used in the weighting for image construction. Finally, in the case that exactly 1 image remains following any exclusion protocol, this is taken to be the successfully identified image.

IV. RESULTS

A. Image Retrodiction

Fig.s 7a and 7b show the retrodicted image of the portrait of Emmy Noether after 1 and 1000 time steps, with values of $Q = 0.75$ and $Q = 770.79$, respectively. After one time step - one measurement and retrodiction calculation - the brighter pixels occur where a photocount was measured. After 1000 time steps, 1000 state retrodictions, the transmitted image is clear.

B. Letter Recognition

For each letter, the transmission and identification procedure was trialled 500 times. The accuracy of identification was 95.8% for 1 time step, for only 3 letters it was less than 100%, B,D and T. For 2 time steps, B and D were found 100% of the time and for T, 3 time steps were necessary for 100% reliability. The average value for photocount per pixel with correct identification was $\bar{Q} = 0.28$ for 1 time step, $\bar{Q} = 0.54$ for 2 steps (B and D) and $\bar{Q} = 0.99$ for 3 (T). Fig.s 8a and 8b show the measured image for letters I and T after 1 time step.
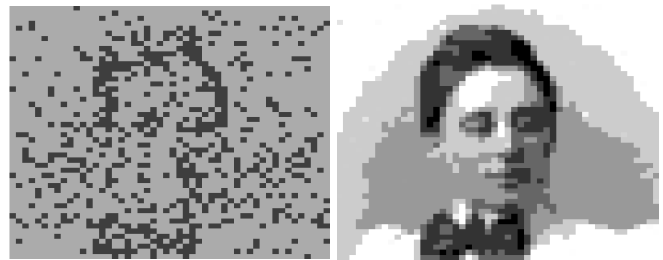
(a) 1 Step Noether portrait retrodiction   (b) 1000 Steps Noether portrait retrodiction

FIG. 7: Retrodicted portrait of Emmy Noether after (a) a single time step or (b) 1000 time steps. After a single retrodiction, locations where a photocount occurred are imaged brighter than those where no count was measured. After 1000 retrodictive upadates the light state is refined and clearly depicts the portrait of Emmy Noether.

(a) 1 Step 'I' retrodiction   (b) 1 Step 'T' retrodiction

FIG. 8: Single time step image retrodictions for letters (a) I and (b) T. Brighter pixels indicate brighter states due to photocounts. The image for T shows that the occurrence of a photocount to exclude I from the base is unlikely, as the location of the I corresponds to the vertical bar of the T. However, photocounts in the I image at the location of the T's crossbar will exclude the T from the base when an I is transmitted.

C. Portrait Recognition

For each of the portrait library images, the transmission and identification simulation was trialled 500 times. The average value for Q was determined for correctly identified images, $\bar{Q} = 0.65$ with a standard deviation $\sigma_{\bar{Q}} = 0.08$. Fig. 9 shows how the value for Q for each image varied with the brightness of the image. The red curve is the click probability $P(\checkmark|\bar{n}) = 1 - e^{-\eta\bar{n}}$ (Eq. (16)) with which Q versus average brightness is expected to follow.

Transmitted portraits were correctly identified or formed 98.32% of the time with standard deviation 0.79%. The accuracy of the double 2σ exclusion process was 100% for image identification (a single image remained), which occurred for 95.81% of all runs with a standard deviation of 0.68%. The double 2σ exclusion
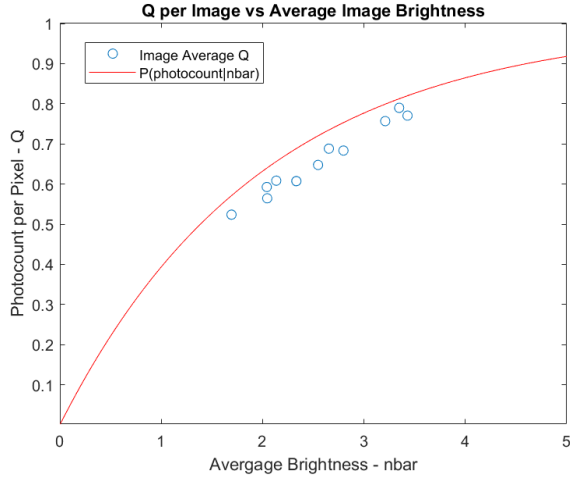
FIG. 9: Average photocount per pixel Q for each portrait library image versus average library image brightness. The red line indicates click probability given mean photon number, $P(\checkmark|\bar{n})$. The images all lie below this red line as only a single photon can be detected per pixel per time step regardless of the brightness at the pixel.

did not leave more than 1 image in any trial nor in any of thousands of runs in development of the algorithm, emphasising the rarity of this event.

1. Image Formation

Weighted image formation occurred for 4.19% of trials, the procedure had accuracy 58.76% with a 21.47% standard deviation. The success of image formation varied greatly depending on the image and method. Exclusion by black and $G1$ comparison then weighting provided an accuracy of 77.03% with a standard deviation of 30%. For some images accuracy was 100% and others as low as 7%. As image formation took place rarely (approximately 20 trials for each image) this data is likely to be not indicative of the true capacity. Image construction following only black pixel comparison never returned the correct image. Fig.s 10,11a and 11b show representative instances of image formation for each of the methods. 2 are presented for the case of formation following $G1$ exclusion (Fig.s 11a and 11b) to display the varying quality. The image formed following black pixel exclusion (Fig. 10) is representative of those produced by this protocol, though many provide less distinct images i.e. more blurred.

D. Single 2σ Exclusion

A single 2σ exclusion was run for each pixel shade and transmission of each library image 100 times. Table I dis-

FIG. 10: Image formation following transmission of John von Neumann's image. This image was formed after the the $G1$ pixels excluded all images from the basis and those remaining after the black pixel exclusion are weighted according to the measured image data by the process in Sec. III D
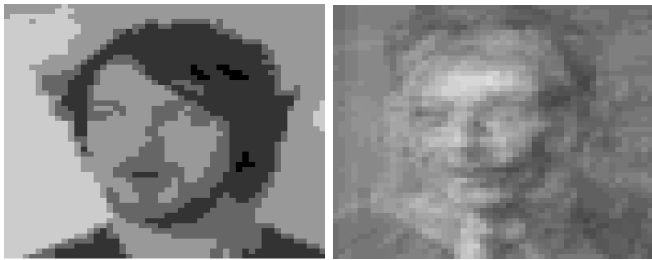

(a) Good image formation   (b) Bad image formation

FIG. 11: Image formation following transmission of John von Neumann's image. These were formed after $G4$ pixels excluded all images in the basis and those remaining after black and $G1$ pixel exclusion were weighted. (a) presents a successful formation and (b) an unsuccessful image formation, looking instead like Richard Feynman. The difference in quality is a result of the statistical variation in photocount measurements.

plays the average number of images remaining following the exclusion protocol with the accuracy (how often it left only the transmitted image in the basis).

TABLE I: Data from a single 2σ exclusion for each shade (excluding black). Average number of basis images remaining and accuracy (how often the only remaining image was the transmitted image) were taken 100 times for each portrait library image.

	G1	G2	G3	G4	White
Average remaining	1.36	11.66	8.28	4.30	8.3
Accuracy (%)	67	3.2	8.7	16.95	0

(a) Transmitted non-library image

(b) Image formation of non-library image

FIG. 12: The transmission of a non-library image (a), the author of this paper, resulted in the formation of (b), the weighting of non-excluded images. There faint resemblance to a face is unsurprising given the image is constructed from only images of faces.

E. Non-Library Member Identification

Finally, an image of a non-member of the portrait library (the author of this paper) was processed by the algorithm, Fig 12a. Figure 12b is representative of the resulting image formation - no member of the library was falsely identified in any of 500 trials.

V. DISCUSSION

A. Photocounts Per Pixel and Brightness

Given a single time-step, a sub-unity value for Q was expected. In 1 time-step, each detector produces only a binary detection determined by Eq. (16) and some detectors will not click, due to either a dark source, statistical nature of photon occurrence or the imperfect detection efficiency. As expected, Q varied with the average brightness of the image, displayed in Fig. 9. The red curve is the click probability $P(\checkmark|\bar{n}) = 1 - e^{\eta\bar{n}}$. As seen, the values for Q are all lower than the red curve for the same brightness. This results from the dead time of the detectors allowing only 1 photocount per detector per time step regardless of the brightness of the state.

The retrodicted portrait of Emmy Noether (Fig. 7b) emphasises the improvement of image identification for low photon imaging. The Q value is a factor of 1000 larger than that necessary for the double 2σ identification procedure.

Photocounts in each time step provide evidence for a retrodictive refinement of the mixed state of the light source. The algorithm then asks, for each library image: does the brightness of the state (measured image) in a particular region match the expected brightness for this image? Large deviations from what is expected exclude the base image as a candidate for identification and smaller deviations provide a measure of dissimilarity. As discussed, a single time step image identification is highly reliable for both libraries and 100% effective with a few more time steps for the alphabet library. Further time steps provide further refinement of the pre-measured light state. Development of the software to exploit this for the portrait library could potentially improve the reliability of image identification to near 100%, whilst maintaining a low photocount.

B. Orthogonal Images

The alphabet library provides a simple case for single photon exclusion. The letters are all orthogonal, having overlapping white on black regions sufficient to exclude all other letters. So, the states of light comprising the letters are orthogonal. All that was required were photocounts occurring where enough states are dark to distinguish between 26 images. On average, for the letters B, D and T, the accuracy was less than 100% for 1 time step, meaning more than 1 image remained following the exclusion algorithm. Figures 8a and 8b display the single time step measurement of I and T. As photocounts are used to exclude letters, it is clear that the measured image for T is less likely to provide a photocount to exclude I than an O, for example. The letter T versus I has a very small orthogonal region, which often is not illuminated. It is also likely that the measured image for I will exclude T by a single pixel turning brighter in the cross-bar of the T - explaining why T but not I had a lower accuracy. Likewise, B and D may have trouble excluding each other due to the similarity of shape and therefore the state of light representing them. The portrait library further demonstrates the need for orthogonal regions to distinctly discriminate between images. The black pixel exclusion always left at least 7 images; these 7 have no black pixels and cannot be excluded.

C. Non-Orthogonal Images

Orthogonality necessarily restricts the set of identifiable images. For discernment from a more interesting set of images, statistical interpretation of the measured data was required. The double 2σ exclusion procedure left only one image in the basis for 95.81% of trials, 100% of these were the transmitted image. This offers a highly reliable image identification procedure from a very low photocount per pixel. Thousands more trials were run in experimentation and development of the algorithm and an incorrect image identification never occurred. However, given the statistical nature of the measurements, it is theoretically possible for the procedure to return an incorrect result. For this to occur, not only would the transmitted image need to be excluded, but just a single other base image would have to defy exclusion by both shade considerations. $G1$ and $G4$ exclusion leave averages of 1.36 and 4.30 images respectively (Table I), following exclusion. These combined efficacies explain

the rarity of incorrect identification. The fact that the double 2σ exclusion procedure never left more than one image in any trial, gives further confidence in the identification procedure. If only a single 2σ exclusion took place, then, according to Table I, at best 67% accuracy would be achieved. Further, if more than two 2σ exclusions are used, the occurrence of image formation would increase, reducing the effectiveness of identification. Therefore, the double 2σ exclusion is optimal for non-orthogonal image recognition.

1. Image Forming

Image formation had mixed results depending on the method and image transmitted. The procedure weighting images after black pixel exclusion was unsuccessful, generating undistinct face-like blurred images (Fig. 10). For this there are 2 significant reasons. The image was formed from at least 7 (those remaining after black pixel exclusion) non-standardised images - faces were not in the same location, not facing the same direction and not with the same lighting. Too many different overlapping features blur-out a definite face. Second, from Table I, $G1$ pixels provided the most distinguishing information. In this case, $G1$ exclusion had removed the transmitted image, meaning the measurement for these pixels was outwith 2 standard deviations of the mean. So, the image is constructed regarding the data from the $G2, G3$ and $G4$ pixels, which provide less distinguishing information. This is due to a large overlap for these shades between images, so photocounts for non-corresponding shades are confused.

In contrast, image formation following black and $G1$ exclusion was much more effective with an accuracy of 77.03%. Of the approximately 23% that were wrong (not exactly the same as the transmitted image), many looked very similar to the transmitted image (Fig. 11a). The reason for this is the highly discriminating information of the $G1$ pixels being available. The caveat is that it occasionally returned an image looking like the wrong person (Fig. 11b). This is likely due to the number of clicks at $G1$ pixels for the base image corresponding to the transmitted image deviating far from the expected value, but not sufficiently to exclude it. This results in the transmitted image's base image being weighted weakly in image formation. It may also be the result of the $G1$ pixels having excluded the transmitted image's base image and it not being used in image formation.

In both image formation and image deciding, the quality of results depends on targeting shades that provide highly differentiating information. That is, have expectations for brightness at regions that differ sufficiently such that measurements can distinguish them. Furthermore, they must not overlap too much. As only a single time step measurement was made, distinguishing brightnesses is not possible and photocounts from overlapping shades are confused. Developing this software to take advan-

tage of the contrasting brightnesses from 2 or more time steps offers potential for improving the reliability of the double 2σ excluder without much sacrifice in increasing photocount.

The response to a non-member of the library is to form an amalgamation of library images weighted according to the measured spatial brightness variation. It is not surprising that the formed image is a face. Any received photocount data will be used in weighting the base images that are not excluded and the result is necessarily a face to varying degrees of distinctness. The formed image is not representative of the face image transmitted but rather the similarity of shade region sizes. In the 'eigenface' technique, the faces provide a basis from which, ideally, any face can be constructed. Whilst this was the motivation for the image formation in this work, the images here are far from 'eigenfaces', being collected without standardisation nor decomposition into a basis set. As such, it is not possible that this procedure will form recognisable images of non-members of the library.

D. Photons Per Pixel

While photocounts, in this setup, necessarily indicate photons transmitting the image - dark count was excluded - many transmitted photons are not represented by the value of Q. One reason is the imperfect detectors. Whilst the photocount per pixel value $\bar{Q} = 0.65$ for the portraits, the detection efficiency $\eta = 50\%$. So, the number of photons per pixel might be expected at 1.3. Furthermore, regardless of the brightness of the illuminating state, a detector can only click or not as it becomes insensitive for a duration following activation. This will increase the number of photons unrepresented by Q. The length of the dead time is equivalent to the time step in this work. The duration was unspecified but assumed to be sufficient to permit the relative photocount rate to distinguish intensity. The interplay between a varying detector dead time and Q remains an area for exploration. This method is likely to exclude many more photons than the 50% detection efficiency is responsible for. A more physically realistic simulation might take the form of detection events, running independently from one another (rather than parallel), with a time resolution a fraction of the dead time. This could be combined with a continual analysis of the state to exclude images from the basis until an image is identified.

E. Image Collapse

An interesting reflection inspired by quantum theory may be made for orthogonal images. Pre-measurement, the image can be considered a uniform distribution of the base images. Following the detection of photons that exclude sufficient images, there is a collapse of this superposition of images to one clearly defined base image. If it

is known with 100% certainty that the image transmitted was a member of the basis set (the system hasn't been fooled by photocounts from an unexpected image), then the previously mixed "unknown" state of light is now "known" as a pure state. Discriminating the image, discerns the quantum state. In the case of non-orthogonal images a more refined mixed state is discerned. This poses an intriguing epistemological question. Is the, perhaps unreliable, "knowledge" that a member of the library was transmitted and a few photocounts sufficient to "know" the quantum state of the light source?

VI. CONCLUSION

Inspired by the quantum retrodiction literature and image discrimination techniques, the work presented here adds to the record of sub-unity photocount per pixel ratios. Orthogonal images are shown to be absolutely distinguished by appropriately located photocounts and non-orthogonal images can be discriminated by the difference in number of photocounts in a region (brightness) compared to that expected for an image. Furthermore,

limited photocount data provided some success in forming a weighted image to offer when the transmitted image is not uniquely determined. The reliability and quality of the image discrimination and formation procedures, presented here, are crucially dependent on the differentiating capacity of the image regions targeted to compare brightness expectations and measured data. Taking measurements of greater numbers of time steps for more refined brightness retrodictions can potentially improve the discriminating capacity of this procedure. However, this necessarily requires greater photocounts per pixel. In answer to the need for low intensity imaging techniques, this work presents a reliable and relatively straightforward protocol for image discrimination from low photocount.

To request the full simulation code contact the author by email.

ACKNOWLEDGMENTS

[1] Reuben S Aspden, Nathan R Gemmell, Peter A Morris, Daniel S Tasca, Lena Mertens, Michael G Tanner, Robert A Kirkwood, Alessandro Ruggeri, Alberto Tosi, Robert W Boyd, Gerald S Buller, Robert H Hadfield, and Miles J Padgett. Photon-sparse microscopy: visible light imaging using infrared illumination. *Optica*, 2(12):1049, 2015.

[2] Peter A Morris, Reuben S Aspden, Jessica E. C Bell, Robert W Boyd, and Miles J Padgett. Imaging with a small number of photons. *Nature communications*, 6(1):5913–5913, 2015.

[3] Lena Mertens, Matthias Sonnleitner, Jonathan Leach, Megan Agnew, and Miles J Padgett. Image reconstruction from photon sparse data. *Scientific reports*, 7(1):42164–42164, 2017.

[4] Steven D Johnson, Paul-Antoine Moreau, Thomas Gregory, and Miles J Padgett. How many photons does it take to form an image? *Applied physics letters*, 116(26):260504, 2020.

[5] *Quantum imaging / [internet resource].* Springer, New York, 1st ed. 2007.. edition, 2007.

[6] Rodney Louden. *The Quantum Theory of Light.* Oxford University Press, Great Clarendon Street, Oxford, 2000.

[7] *Advanced photon counting : applications, methods, instrumentation / [internet resource].* Springer series on fluorescence; 15. 1st ed. 2015.. edition, 2015.

[8] Fiona C Speirits, Matthias Sonnleitner, and Stephen M Barnett. From retrodiction to bayesian quantum imaging. *Journal of optics (2010)*, 19(4):44001, 2017.

[9] Stephen M Barnett, Lee S Phillips, and David T Pegg. Imperfect photodetection as projection onto mixed states. *Optics communications*, 158(1-6):45–49, 1998.

[10] Stephen M Barnett, David T Pegg, and John Jeffers. Bayes' theorem and quantum retrodiction. *Journal of modern optics*, 47(11):1779–1789, 2000.

[11] Matthias Sonnleitner, John Jeffers, and Stephen M Barnett. Image retrodiction at low light levels. *Optica*, 2(11):950, 2015.

[12] Curtis J Broadbent, Petros Zerom, Heedeuk Shin, John C Howell, and Robert W Boyd. Discriminating orthogonal single-photon images. *Physical review. A, Atomic, molecular, and optical physics*, 79(3), 2009.

[13] S Franke-Arnold and J Jeffers. Unambiguous state discrimination in high dimensions. *The European physical journal. D, Atomic, molecular, and optical physics*, 66(7):1–4, 2012.

[14] G. Michael Morris. Image correlation at low light levels: a computer simulation. *Appl. Opt.*, 23(18):3152–3159, Sep 1984.

[15] Wojciech Roga and John Jeffers. Efficient location, imaging and recognition of faces by single-pixel camera. *Journal of optics (2010)*, 20(12):125701, 2018.

[16] Durini Daniel. Charge-coupled device (ccd) image sensors. In *High Performance Silicon Imaging - Fundamentals and Applications of CMOS and CCD Sensors*, pages 1–1. Elsevier, 2nd edition edition, 2020.

[17] F Zappa, S Tisa, A Tosi, and S Cova. Principles and features of single-photon avalanche diode arrays. *Sensors and actuators. A. Physical.*, 140(1):103–112, 2007.

[18] Karl-Rudolf Koch. *Introduction to Bayesian statistics / [internet resource].* Springer, Berlin ; New York, 2nd, updated and enl. ed.. edition, 2007.

[19] *Aristotle.* After Lysippos, Public domain, via Wikimedia Commons.

[20] *Niels Bohr.* The American Institute of Physics credits the photo to AB Lagrelius Westphal, book series Les

Prix Nobel., Public domain, via Wikimedia Commons.

[21] *Stephen Hawking.* NASA, Public domain, via Wikimedia Commons.

[22] *Emmy Noether.* Mathematical Association of America Public domain, via Wikimedia Commons.

[23] *Ludwig Boltzmann.* Public domain, via Wikimedia Commons.

[24] *Marie Curie.* Henri Manuel, Public domain, via Wikimedia Commons.

[25] *James Clark Maxwell.* Public domain, via Wikimedia Commons.

[26] *Roger Penrose.* Cirone-Musi, Festival della Scienza, CC BY-SA 2.0, via Wikimedia Commons.

[27] *Louie de Broglie.* Public domain, via Wikimedia Commons.

[28] *Paul Dirac.* Nobel Foundation, Public domain, via Wikimedia Commons.

[29] *John von Neumann.* LANL, Attribution, via Wikimedia Commons.

[30] *Max Planck.* Public domain, via Wikimedia Commons.

[31] *Albert Einstein.* Ferdinand Schmutzer, Public domain, via Wikimedia Commons.

[32] *Richard Feynman.* Public domain, via Wikimedia Commons.

[33] *Isaac Newton.* Public domain, via Wikimedia Commons.

[34] *Ernest Rutherford.* Public domain, via Wikimedia Commons.

[35] *Carl Gauss.* Christian Albrecht Jensen, Public domain, via Wikimedia Commons.

[36] *Sabine Hossenfelder.* HossenfelderS, CC BY-SA 4.0, via Wikimedia Commons.

[37] *Erwin Schrodinger.* Nobel foundation, Public domain, via Wikimedia Commons.

[38] *Nikola Tesla.* Public domain, via Wikimedia Commons.

Appendix A: Coherent Source No-click Probability Derivation

The total probability for a no-click event is the expectation value of the no-click detection operator in the mixed state $\hat{\rho}_\alpha'$ (Eq. 8).

$$P_\alpha(\times) = \langle \hat{\Pi}_\times \rangle \tag{A1}$$
$$= Tr\big(\hat{\rho_\alpha}'\hat{\Pi}_\times\big)$$
$$= \sum_m \langle m| \frac{1}{\bar{m}+1} \sum_{\bar{n}=0}^{\bar{m}} e^{-\bar{n}} \frac{\bar{n}^n}{n!} |n\rangle \langle n| \sum_{n'} (1-\eta)^{n'} |n'\rangle \langle n'|m\rangle$$
$$= \frac{1}{\bar{m}+1} \sum_m \sum_{\bar{n}=0}^{\bar{m}} \sum_n \sum_{n'} e^{-\bar{n}} \frac{\bar{n}^n}{n!} (1-\eta)^{n'} \underbrace{\langle m|n\rangle}_{\delta_{m,n}} \underbrace{\langle n|n'\rangle}_{\delta_{n,n'}} \underbrace{\langle n'|m\rangle}_{\delta_{n',m}}$$
$$= \frac{1}{\bar{m}+1} \sum_{\bar{n}=0}^{\bar{m}} e^{-\bar{n}} \sum_n \frac{(\bar{n}(1-\eta))^n}{n!}$$
$$= \frac{1}{\bar{m}+1} \sum_{\bar{n}=0}^{\bar{m}} e^{-\eta\bar{n}} \tag{A2}$$

Appendix B: Thermal Source Theoretical Considerations

A thermal source of unknown intensity is represented by a uniform distribution of thermal states over mean photon number up to maximum $\bar{m}$.

$$\hat{\rho}_{th} = \frac{1}{\bar{m}+1} \sum_{\bar{n}=0}^{\bar{m}} \frac{1}{\bar{n}+1} \sum_n \big(\frac{\bar{n}}{\bar{n}+1}\big)^n |n\rangle \langle n|. \tag{B1}$$

So, finding the expectation value of the no click operator, Eq. (9), is done analogously as for the coherent state in Sec. II D.

$$P_{th}(\times) = Tr\big(\hat{\rho_{th}}\hat{\Pi}_\times\big)$$
$$= \sum_m \langle m| \frac{1}{\bar{m}+1} \sum_{\bar{n}=0}^{\bar{m}} \frac{1}{\bar{n}+1} \sum_n \big(\frac{1}{\bar{n}+1}\big)^n (1-\eta)^n |n\rangle \langle n|m\rangle$$
$$= \frac{1}{\bar{m}+1} \sum_{\bar{n}=0}^{\bar{m}} \sum_m \frac{1}{\bar{n}+1} \underbrace{\sum_n \big(\frac{\bar{n}(1-\eta)}{\bar{n}+1}\big)^n}_{\sum_n x^n = \frac{1}{1-x}} \underbrace{\langle m|n\rangle}_{\delta_{m,n}} \underbrace{\langle n|m\rangle}_{\delta_{n,m}}$$
$$= \frac{1}{\bar{m}+1} \sum_{\bar{n}=0}^{\bar{m}} \frac{1}{\bar{n}+1} \frac{1}{1-\frac{\bar{n}(1-\eta)}{\bar{n}+1}}$$
$$= \frac{1}{\bar{m}+1} \sum_{\bar{n}=0}^{\bar{m}} \frac{1}{1+\eta\bar{n}} \tag{B2}$$

Recalling Eq. (5) the total probability for no click,

$$P(\times) = \sum_{\bar{n}} P(\times|\psi_{\bar{n}}) \cdot P(\psi_{\bar{n}}). \tag{B3}$$

The comparison is made as in the main text, Eq.s (B2) and (B3). The prior is $P_{th}(\bar{n}) = \frac{1}{\bar{m}+1}$, the predictives are $P_{th}(\times|\psi_{\bar{n}}) = \frac{1}{1+\eta\bar{n}}$ and $P_{th}(\checkmark|\psi_{\bar{n}}) = 1 - \frac{1}{1+\eta\bar{n}}$.

Appendix C: Image Retrodictor Demonstration

The following simple image (Fig. 13) was supplied to the algorithm. It was retrodicted assuming either a co-
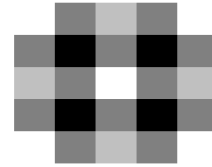

FIG. 13: Simple image input to retrodicton algorithm.

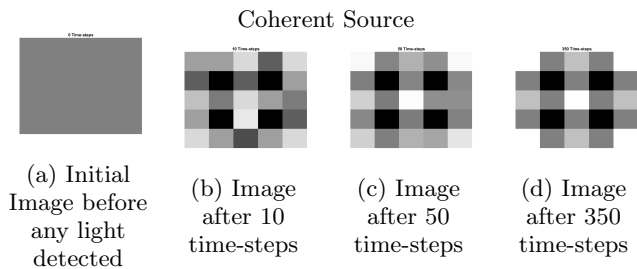herent (Fig. 14) or thermal source (Fig. 15) for comparison.

Coherent Source

(a) Initial Image before any light detected

(b) Image after 10 time-steps

(c) Image after 50 time-steps

(d) Image after 350 time-steps

Thermal Source

(a) Initial Image before any light detected

(b) Image after 10 time-steps

(c) Image after 50 time-steps

(d) Image after 350 time-steps

FIG. 14: (a) an image of the initial uniform prior, all pixels are grey as there is no information to indicate spatial variation of light. (b) the image is beginning to emerge but the intended image is still unclear. (c) repeating bayesian updates are refining the prior and the image is nearly discovered. (d) by 350 time-steps, enough information has been incorporated by bayesian inference to determine the spatial variation of brightnesses. This is in contrast with Fig. 15d for the thermal source below, where the image is still not fully revealed after 350 time-steps
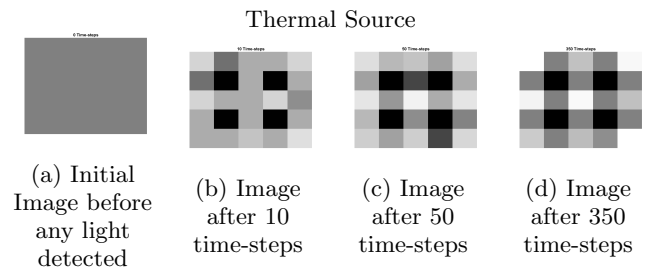
FIG. 15: (a) an image of the initial uniform prior, all pixels are grey as there is yet information to indicate spatial variation of light. (b) the image is beginning to emerge but the intended image is still unclear. (c) repeating bayesian updates are refining the prior and the image is nearly discovered. (d) by 350 time-steps, the image is still not fully revealed. This is in contrast to Fig. 14d above for the coherent source, where the image is fully revealed by the same number of time-steps.

The initial image (uniform prior) and resulting images after 10, 50 and 350 time steps for each source are presented below.

Figure 16 shows the evolution of the brightness of each pixel over the retrodiction process for each light source. The thermal state is seen to require approximately 5 times as many time steps for equivalent image retrodiction. Both resulting images required thousands of photons per pixel.
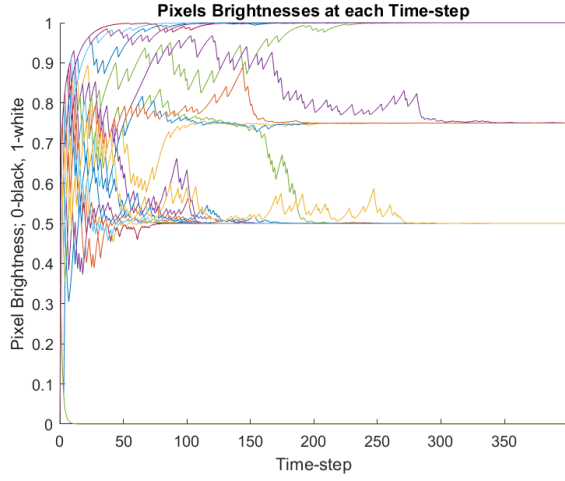
(a) Coherent state pixel brightness evolution over 400 time-steps.
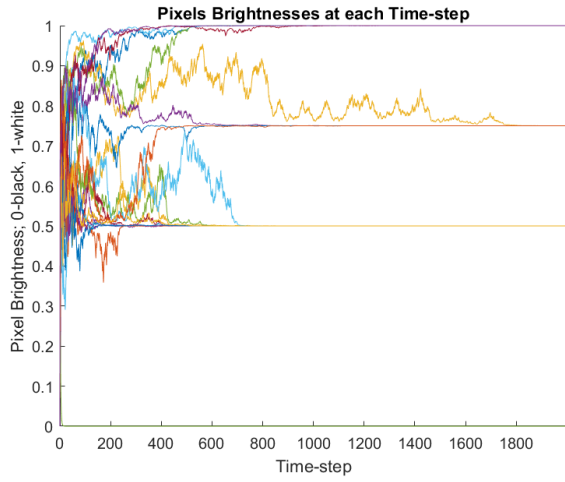
(b) Thermal state pixel brightness evolution over 2000 time-steps.

FIG. 16: In both (a) and (b), there is, at first, ostensibly chaotic variations in brightness at the different pixels. With sufficient steps, convergence to particular brightness values, $0, 0.5, 0.75, 1$ corresponding to input $\bar{n} = 0, 2, 3, 4$ respectively is seen. For the coherent source (a), this convergence occurs much sooner, by approximately 150 steps, becoming sharp by 300. (b) the thermal source, is still very unpredictable after the same number of time-steps but a tentative convergence is apparent after 900 steps and is not sharply defined until 1800 steps.